Advanced Physics Lab SS19

Experiment: Nuclear spin

(conducted on: 10.-11.9.2019 with Stephen Jiggins)

Erik Bode, Damian Lanzenstiel
(Group 103)

September 30, 2019

Abstract

Contents

1 Theory

The contents of this chapter are, if not otherwise specified, derived from the guide to the experiment [2]

1.1 Spin and nuclear spin

The spin or intrinsic angular momentum of a elementary particle is an intrinsic property of particles from the family of the fermions. Members of this family, such as protons, neutrons and electrons all have a spin of $s = \frac{1}{2}$. The spin can be explained semi classically, as rotation of the particle around its own 'centre of mass', with fixed frequency and variable axis of rotation. However, this illustration only makes sense in finite-size particles, of course. Just as with the angular momentum, not all three spin components can be defined at the same time, but only the amount and projection on a freely selectable 'quantization axis'. The possible spin quantum numbers are

$$\left|\vec{S}\right| = \hbar\sqrt{S\,(S+1)}$$

with $S = 0, \frac{1}{2}, 1, ...$ and Planck's constant $\hbar$. Atomic nuclei are also assigned a spin, the nuclear spin, which is defined with the nuclear spin number I, analogue to the spin:

$$\left|\vec{I}\right| = \hbar\sqrt{I\,(I+1)}$$

The nuclear spin number is also quantified in its direction. Analogue to the electron spin, the projection of the nuclear spin can also assume certain states as , e.g. with the z-axis as the quantization axis $I_z = m_I\hbar$ with $-I \leq m_I \leq +I$. In total there would be $2I + 1$ different states for I_z. Protons or the nucleus of ^{19}F both have a nuclear spin number of $I = \frac{1}{2}$. So both have only two possible states: $m_I = \pm\frac{1}{2}$. They can only align parallel or antiparallel with the quantization axis in the experiment.

1.2 Magnetic momentum

The spin of a quantum mechanical particle is connected to a magnetic dipole momentum $\vec{\mu}$, the ratio of both is described as the gyromagnetic ratio γ.

$$\vec{\mu} = \gamma\vec{I} \qquad \text{with} \quad \gamma = \frac{g_I\mu_K}{\hbar}$$

The constant g_I is the nuclear g factor, which is to be calculated during the exam. g_I has no dimension and is unique for each nucleus. The second constant μ_K is the nuclear magneton, which is computed analogue to the Bohr magneton:

$$\mu_K = \frac{e\hbar}{2m_p}$$

The difference between those two is that for the Bohr magneton the elecron mass is used and for the nuclear magneton the proton mass. In the ground state of atomic nuclei, the nucleons are arranged according to the Pauli principle so that each orbital is occupied by two protons or neutrons of opposite spins. If now a eu-nucleus (with an even number of protons and an uneven number of neutrons) or if an ue-nucleus (where the even and uneven nucleons are reversed) is present, an unpaired nucleon remains. This leads to an half-digit total spin. For a uu-nucleus two unpaired nucleons remain resulting in an integer total spin. In a ee-nucleus all nucleons are paired, therefore the total spin is zero. Examples for ee-nuclei are $^{16}_{8}$O and $^{12}_{6}$C. Therefore it is possible to measure the spin of hydrogen $I = \frac{1}{2}$ utilizing glycol ($C_2H_6O_2$) and water (H_2O) samples. For the $^{9}_{19}$F nucleus with 9 protons and 10 neutrons the total spin is also $I = \frac{1}{2}$.

1.3 Interaction with magnetic fields and radiation (nuclear magnetic resonance)

Classically the the energy of a magnetic dipole moment $\hat{\mu}$ in a magnetic field B is described by the equation 1.

$$E = -\hat{\mu} \cdot B \tag{1}$$

If the magnetic field goes in the z direction this can be written in quantum mechanics like in equation 2 and is called Zeeman-splitting.

$$E = -\mu_K g_I m_I B_x \tag{2}$$

Here the energy niveaus are degenerated if there is no outer magnetic field, with the magnetic field the levels spits up depending on the quantum number m_j. In figure 1 we see this splitting up under the influence of the magnetic field.

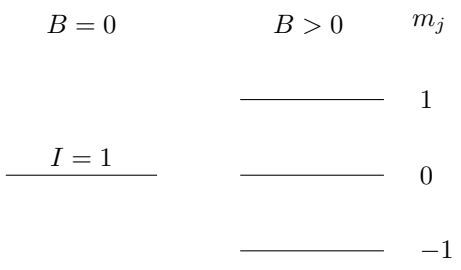

Figure 1: Zeeman splitting for $I = 1$

The difference energy ΔE between attached m_j can be written as follows:

$$\Delta E = g_I \mu_K B \tag{3}$$

This amount of energy needs to be absorbed or emitted for the spin to change its direction. This can happen through photons or by interaction with a 'Strahlungsfeld'. Since a certain amount of energy is needed it happens only at certain frequencies. This so called resonance frequency is given by:

$$\nu = \frac{\Delta E}{h} = \frac{g_I \mu_K B}{h} = \frac{\gamma B}{2\pi} \tag{4}$$

If a spin absorbs energy of the 'Strahlungsfeld' and changes into a higher level the intensity of 'Strahlungsfeld' decreases which is measurable.

2 Relaxation Effects

In thermal equilibrium the occupation number are Boltzmann distributed. The probability of a state depending on energy and temperature is given through:

$$p_i = \frac{e^{-E_i/kT}}{Z} \tag{5}$$

Here k is the Boltzmann constant and Z is the canonical partition function of all the states in the system. The probability p_i can also be given by:

$$p_i = \frac{N_i}{N}$$

With that the relationship between two states 1 and 2 is given through eq.6

$$\frac{N_1}{N_2} = e^{-\frac{E_1 - E_2}{kT}} = e^{-\frac{\Delta E}{kT}} \tag{6}$$

That means that there will always be more particles in the lower state than in an upper one. It follows as well, that the occupation numbers should equalize and with it the measurable effect. This is not happening because of so called relaxation effects. There are two major relaxation effects:

1. Spin-Lattice Relaxation: Here the exited nucleus give their energy to the lattice structure of the molecule. This energy is lost to the 'Strahlungsfeld'.

2. Spin-Spin Relaxation: One nucleus creates a magnetic field at the another nucleus which shifts the outer magnetic field increasing or decreasing it. This leads to an change in the width of the absorption line.

3 Hall Sensor

The Hall sensor is used to measure magnetic fields. It uses the Hall effect. The effect happens to electrons in a cable effected by a outer magnetic field. Here the electrons are pushed under the Lorenz force $\vec{F_L} = q \cdot (\vec{v} \times \vec{B})$ to the side of the cable till certain voltage is reached which counters the Lorenz force $F_L = F_E$. This voltage U_{Hall} can be measured. Equation 7 gives a relationship between the Hall voltage and the magnetic field.

$$U_{Hall} = H\frac{IB}{d} \tag{7}$$

- H: Is the Hall constant $\frac{1}{ne}$ with n the electric charge density and e the charge of an electron.
- I: The current.
- B: The magnetic field.
- d: The width of the cable.

3.1 Lock-in Amplifier

The lock-in method is used to make small signal visible inside of huge noise. To do this the main signal will be multiplied with a reference signal and integrated with a low pass filter and amplified.

4 Method of Measuring

4.1 Measuring the Magnetic Field

To measure the magnetic field the earlier discussed Hall sensor is used. It is put onto a long rod which a cm scale. That way it can be put into the magnetic field and measure it for certain depths. When the magnetic field doesn't change while changing the position of the Hall sensor the field is homogeneously.

4.2 Measurement of the Resonance Frequency

To measure the resonance frequency the constant field method is used. Here the 'Strahlungsfeld' of the NMR (Nuclear Magnetic Resonance) Oscillator is set at a constant frequency and the magnetic field is changed with a wave to check for the correct resonance frequency. If this frequency is hit the spins will change and the 'Strahlungsfeld will lose energy which can be seen in the change of the amplitude. For the magnetic field two electromagnets are used which have to smaller ones attached to vary the field with the help of a wave. To measure the correct frequency two different methods are used.

4.2.1 Sine Modeling Method

The first one uses a sine wave to change the magnetic field. That means that the correct frequency will be hit two times each sine period and with this two absorption lines. To find the exact resonance frequency the minima need to be equidistant, since at this point they will be at the 'Nulldurchgang' of the modulated magnetic field. At this point the correct frequency to the set magnetic field is found. The experimental setup for this part can be seen in figure 2.

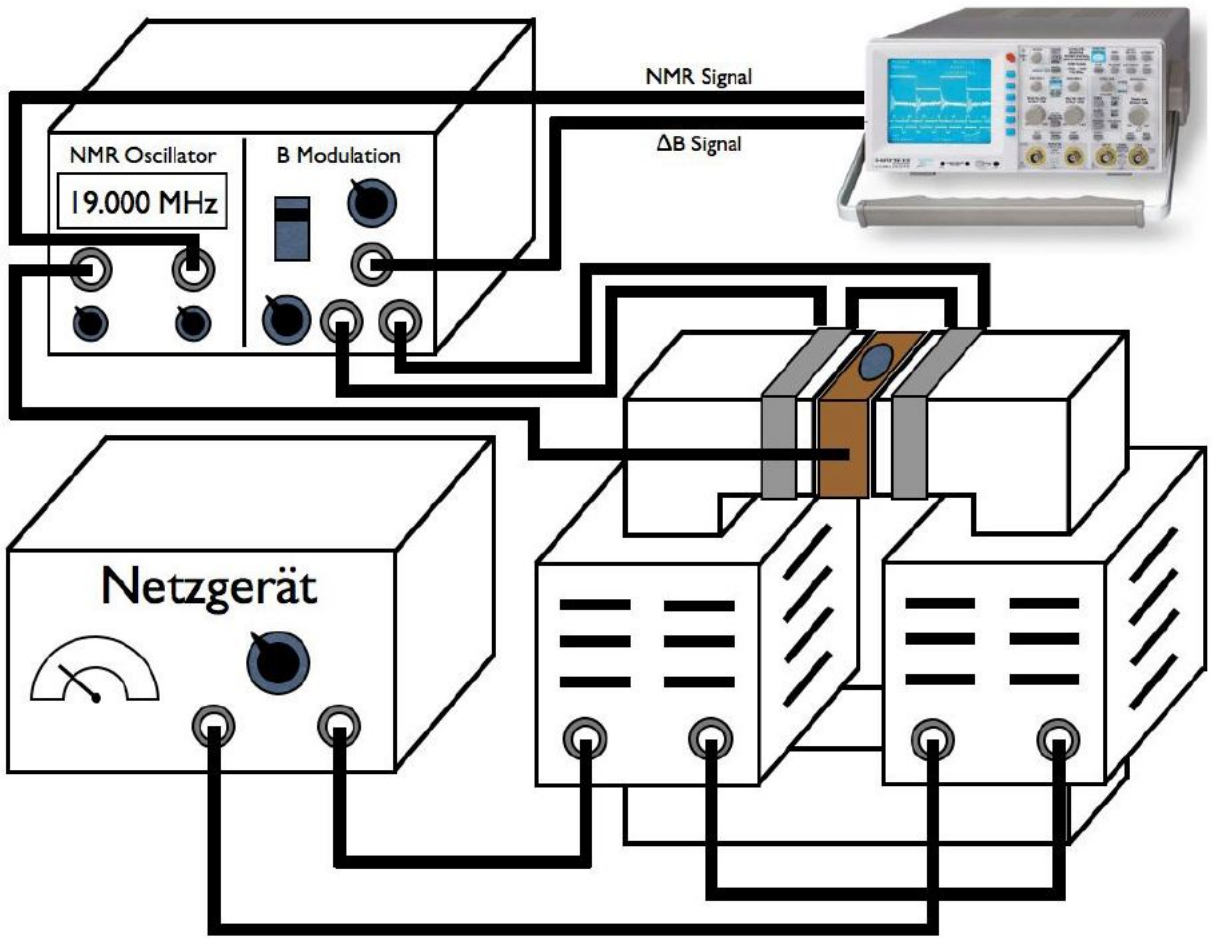

Figure 2: Setup for measuring the resonance frequency with a sine modulation.

4.2.2 Lock-In Method

For the second part the lock-in method is used since it is more precise duo to its lower background noise. Instead of the former absorption curve this method gives the differentiated curve. For the modulation of the magnetic field the superposition of a sine and a sawtooth is used. Here the sawtooth is used mainly for the variance of the field while the sine is used to create the differentiated signal since it has a similar frequency to the reference signal. The former minima of the absorption curve will now be the 'Nulldurchgang' of the signal. The moment the 'Nulldurchgang' of both measured signals overlap the correct resonance frequency is hit. Examples of both signals are shown in figure 23 and the setup is given in figure 3.

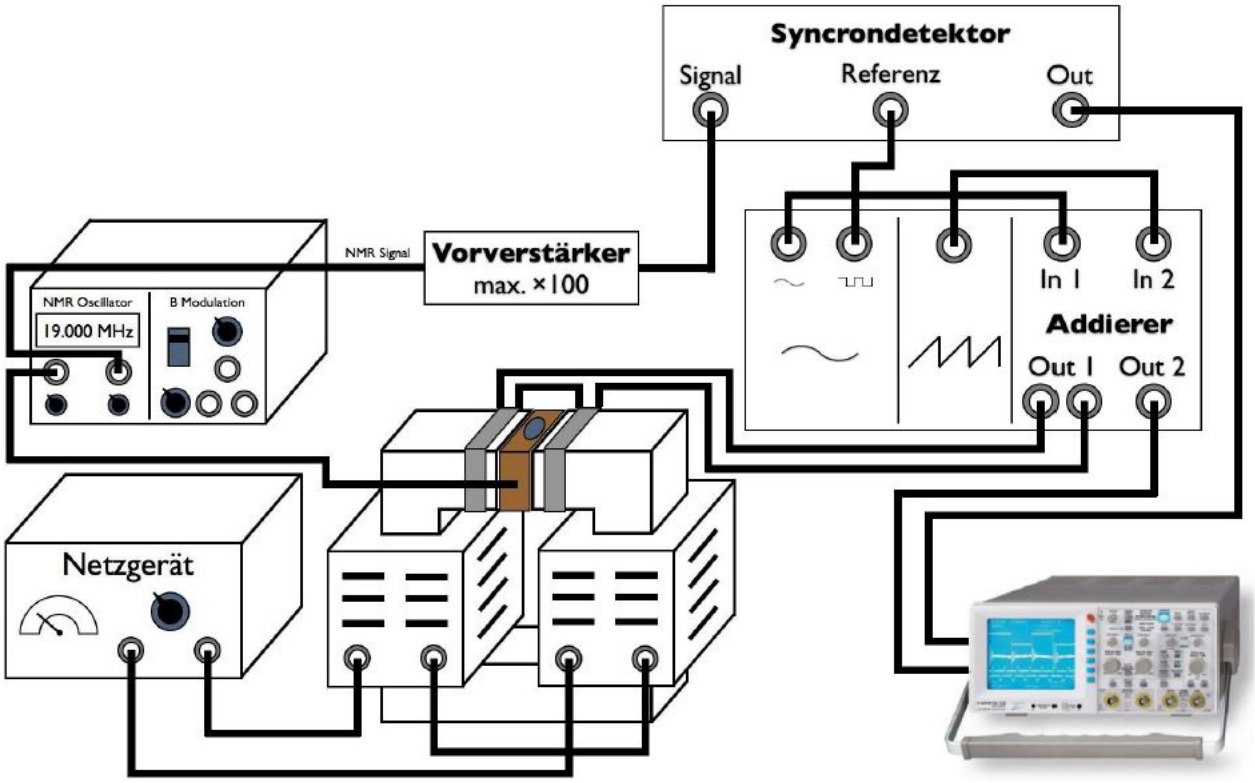

Figure 3: Setup for measuring the resonance frequency with the lock-in method.

5 Conduct of the Experiment

In the beginning of the experiment it had to be checked if the magnetic field inside the setup is homogeneously distributed. For this a Hall-Sensor was used with which the field strength can be measured. Here by the sensor was slowly put into the field and depending on place the strength of the field was recorded. After conforming the uniformity of the field, a position in the middle of the homogeneous part was chosen to place the samples into.

With this set the experiment was set up like in figure 2 described. The measurement was started with the Glycol sample at a depth of 2 cm and a constant magnetic field of 425 mT. With this set, the corresponding frequency of the nuclear magnetic resonance (NMR) oscillator was set by looking for the absorption peaks in the oscilloscope. After learning that it would be easier to find the rough position with a fixed frequency it became much easier to locate the peaks. The fine positioning was still done by modifying the frequency. By setting all peaks equidistant to one another the correct resonance frequency could be found. After this two underground samples were made, one without the H_1 sample inside the field and by setting wrong combinations of magnetic field and oscillation. The H_1 sample was used for all background measurements as well as for the calibration between the change in frequency and the change in position on the oscilloscope. The reason for using H_1 is that it has the least amount of disturbances. It is so to speak our standard candle. With the position - frequency calibration done the actually measurements were started anew. For different combinations of magnetic field and frequency with equidistant absorption lines, the CSV files were taken. After doing this for H_1 and Glycol the Hall-Sensor broke and another one had to be used. This one had the problem that it was strongly influenced by the temperature. This showed by the slowly decrease in measured field strength. The first value measured around the depth of 2 cm was noted.

After finishing this way the ^{19}F sample the Lock in Method was used to decrease the background noise. After building the setup of figure 3 a suitable resonance frequency was chosen. Here a slow shifting of the absorption peaks was noted, most likely duo to the heating of the magnets. After waiting for them to be warmed up the shifting stopped and the first measurement with the Lock in Method could be started. Here a new calibration of position and frequency was made by shifting the positions of the differentiated absorption signal.

Duo to some problems with the measurement of the magnetic field some measurements to the influence of the Hall-Sensor were made. One with the sawtooth voltage and one without it. With these and the voltage and ampere used to create the magnetic field, the accuracy of measurement with the new Hall-Sensor can be determined more closely.

6 Hall Sensor

For the measurement of the homogeneity of the field the data points were plotted in figure 4. It can be seen clearly that after a depth of 7 mm inside the field no change is noticeable so our field is uniform at this point.

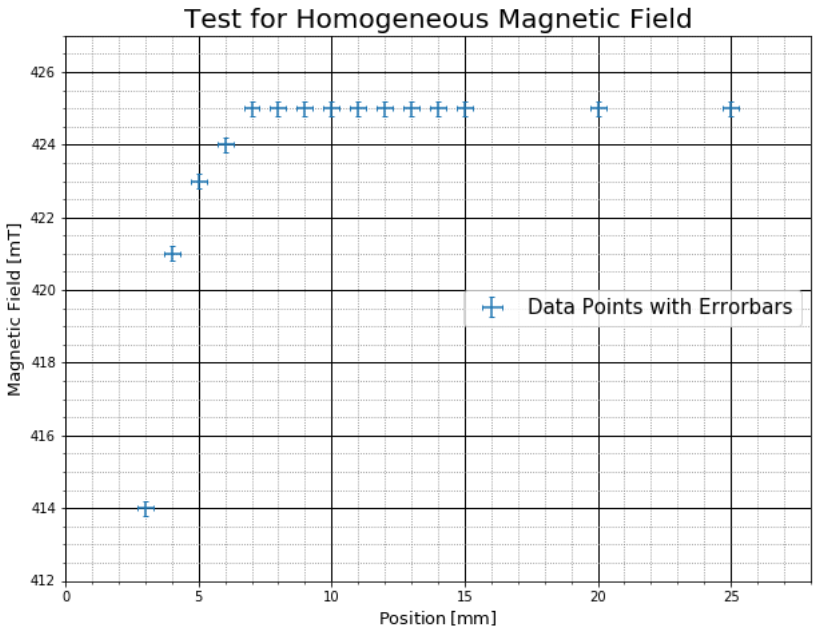

Figure 4: The strength of the magnetic field depending on the depth inside the field.

Since the first Hall sensor was destroyed during the experiment another one had to be used. This one showed a change in the magnetic field depending on the time it was inside the field. To increase the accuracy of the experiment this change was measured once with the sawtooth and once without it. These two can be seen in figure 5 and 6. It is clearly visible that time has an impact on the measurement. In fig.5 we the that for once the change from the sawtooth which slowly decreases the magnetic field and than increases it suddenly. In fig.6 the saturation of after a certain time is seen. It is very likely that the temperature inside point of measurement changes the properties of the Hall sensor. With that it is not clear which is the correct magnetic field. The one at the saturation or the beginning when the sensor is close the room temperature. Inside the manual of the electro magnets a hysteresis curve was found giving the magnetic field depending on the amperage.[1] Since the amperage during the measurement was at 3.41 A the magnetic field strength should be around 415,mT. This value is not very precise since the curve could have changed over time but it clearly shows, that the saturation value is more precise. Since the upper one was used for the measurements, a large systematic error has to be expected for all measurements taken with the new Hall sensor.

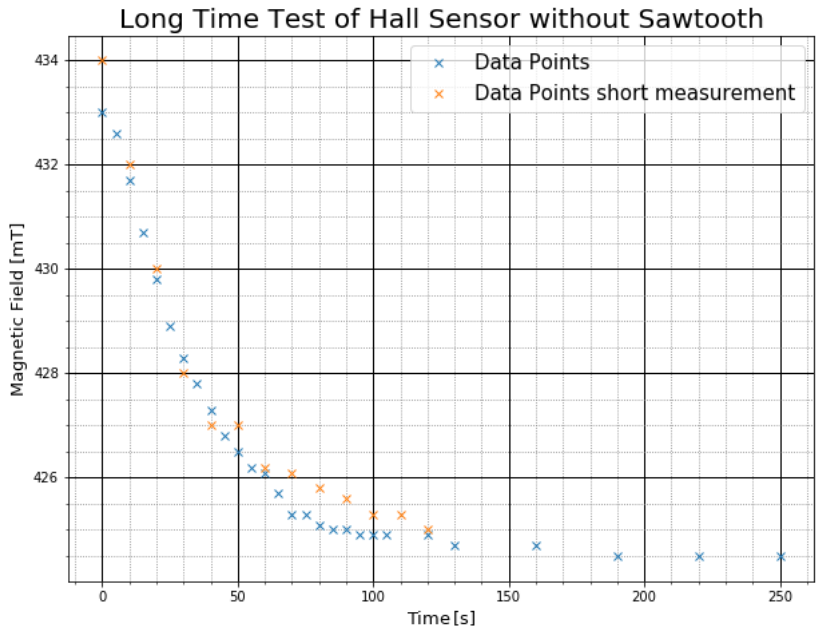

Figure 5: Measurement of the magnetic field depending of the time inside the field with the sawtooth shaped signal. The errors for the data points were to small to make them clearly visible.

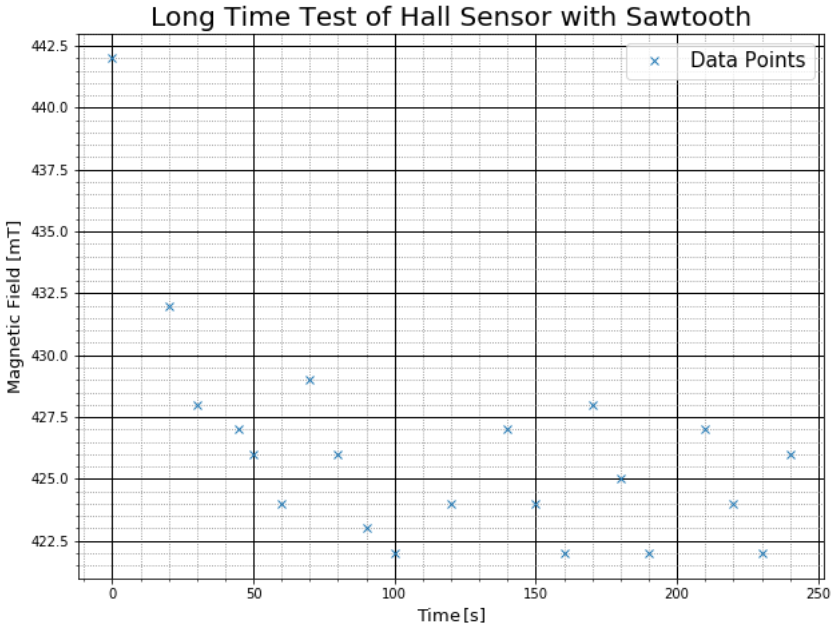

Figure 6: Measurement of the magnetic field depending of the time inside the field without the sawtooth shaped signal. Here two measurements were made one in orange the other one in blue. The errors for the data points were to small to make them clearly visible.

7 Analysis of the sine modeling method

The analysis of the sinus method consists of multiple parts: First the error threshold was computed, which will be used to determine the first absorption dip from each of the change of channels per change of frequency measurements. Second, the change of channels per change of frequency was computed. Third, the actual resonance frequency for each measurement was computed with the relation of the second step of this part of the analysis. Fourth, the combination of the measured magnetic fields and computed frequencies was used to compute the magnetic momentum of the proton in ^{19}F and the gyromagnetic ratio of the proton in glycol and hydrogen.

7.1 Error thresholds

For the error thresholds, one has to take a closer look at the recorded data. The .csv files obtained during the experiment contain the maxima and minima of the curves seen on the oscilloscope. To get a limit which is useful to discriminate the data multiple preparatory steps were necessary: First the absolute values of the differences from two neighbouring background data points were computed and projected to the y axis. A Gaussian curve was fitted to this projection. The maximum of the fitted curve, subtracted from to the mean of the background data used for the projection was the lower error threshold.

In comparison to the out sample or in sample of frequency background, the background during the actual measurement is the most representative, because it was obtained during the exact same conditions as the signal data. After taking an initial look at the measurements used for the frequency difference per channel difference (as seen in fig. 7), it was decided that a sufficient amount of background data points can be obtained from these measurements.

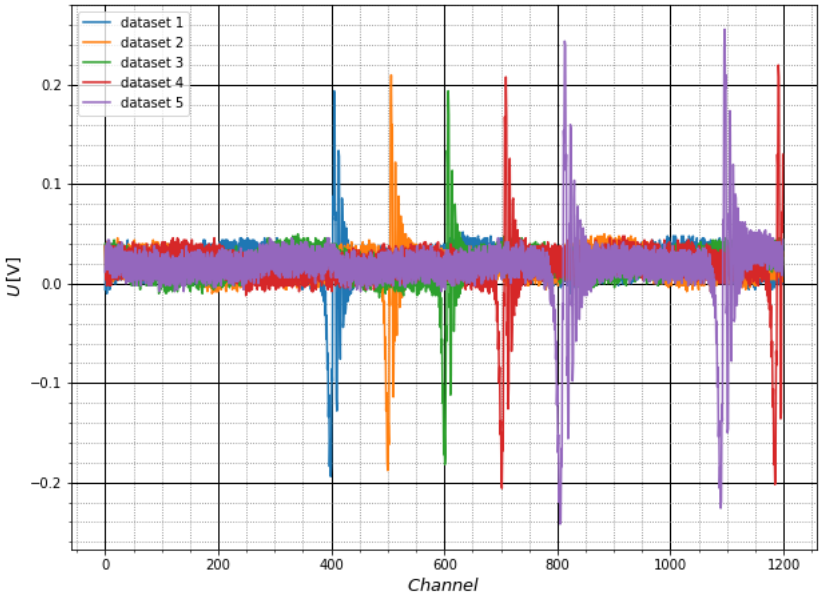

Figure 7: Plot of the measured voltage against the channel of the data points from all five measurements used for the difference in frequency per difference in channel.

After examining the first absorption peak of the first dataset, the parameter to coarsely seperate the background from the absorbtion signals was determined to be $-0.03\,\mathrm{V}$. Both can be seen in fig. 8. All values up to the tenth value underneath this threshold are considered as background signal.

All of these values can be seen in fig. 9. Now, the absolute difference between two neighbouring points was computed, which can be seen in fig. 10. It is clearly visible, that all the data points in fig. 9 and absolute differences in fig. 10 come in discrete levels. The reason behind this is the limited resolution of the analogue digital converter in the oscilloscope, which represents the values as binary numbers of a certain length, allowing only discrete voltage levels to be displayed. These discrete levels result in zeros

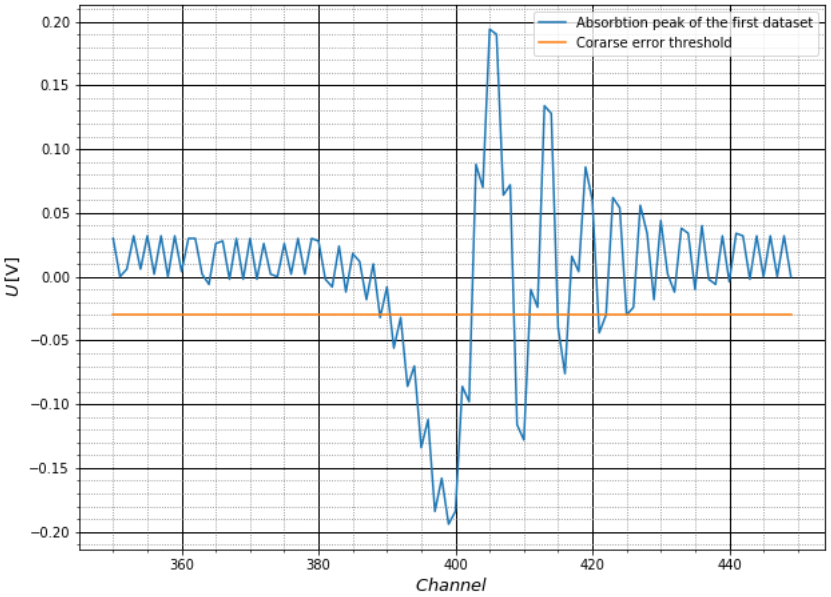

Figure 8: Plot of the measured voltage against the channel of the absorption peak of the first measurement taken for the frequency change channel change ration measurement series. Also seen is the coarse error threshold of $-0.03\,\mathrm{V}$.

in the projection of the values to the y axis, which were not included in the fit of the Gaussian curve. The variance of the fitted Gaussian curve of figure 11 then was subtracted from the mean value of the background data, resulting in the lower error threshold seen in figure 12.

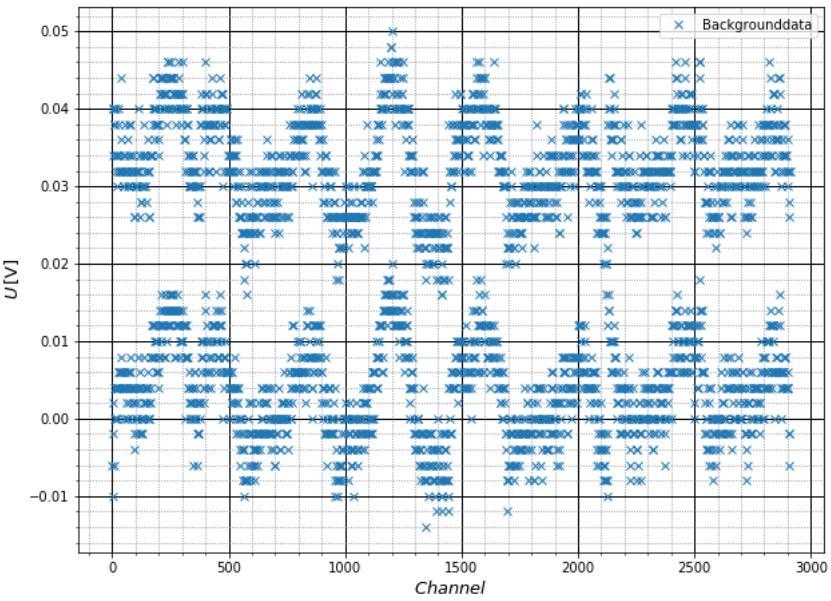

Figure 9: Plot of the measured voltage against the channel of all datapoints used for the error calibration. The discrete voltage levels from the analogue-to-digital converter of the oscilloscope are clearly visible.

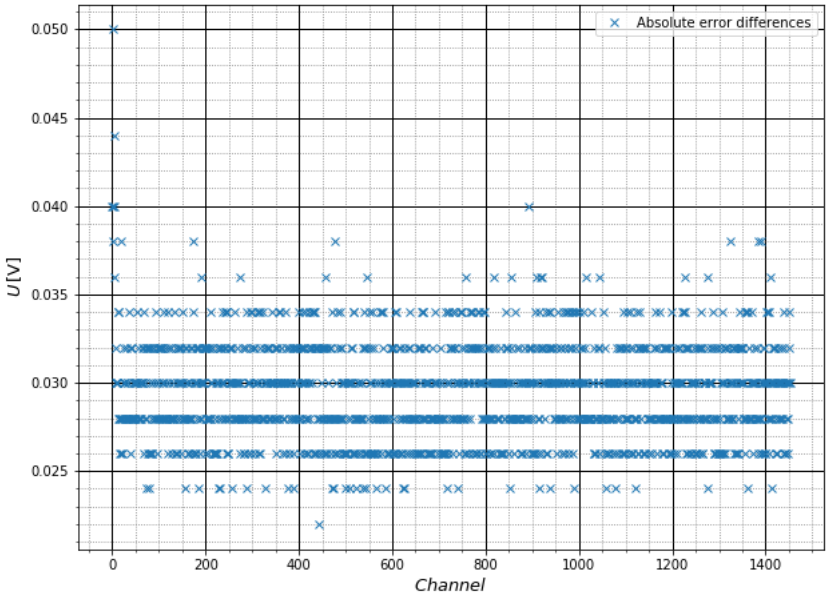

Figure 10: Plot of the measured voltage against the channel of the absolute difference between two neighboring errorpoints from fig. 9. he discrete voltage levels from the analogue-to-digital converter of the oscilloscope are clearly visible.

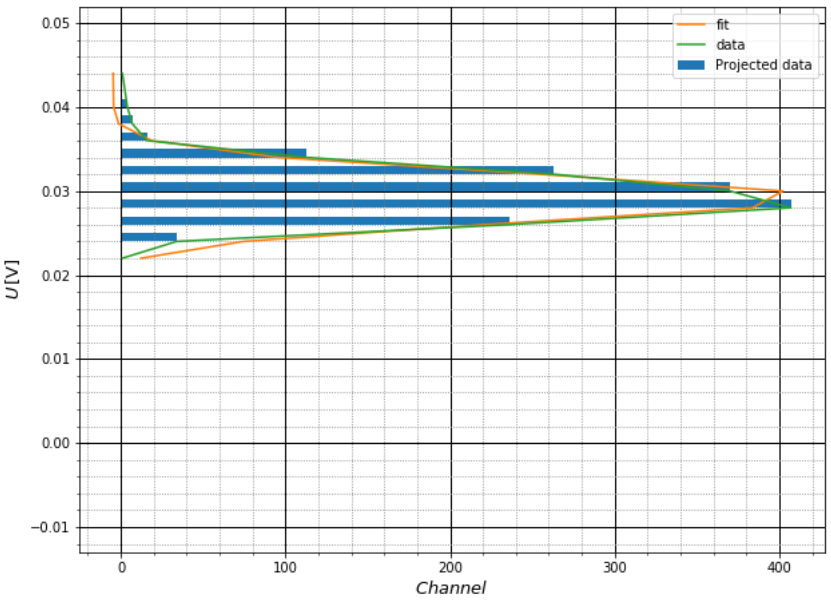

Figure 11: Plot of the projection of the absolute difference between two neighbouring errors to the y axis and the Gaussian curve fitted to them.

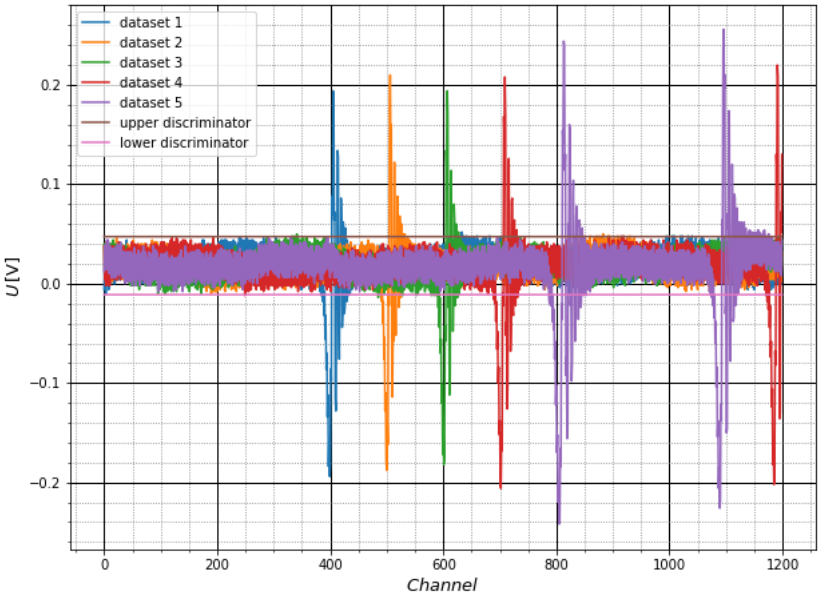

Figure 12: Plot of the measured voltage against the channel of the data points from all five measurements used for the difference in frequency per difference in channel. Additionally, the upper and lower error discriminator are plotted in the figure.

7.2 Computation of the relationship between a change in channels and a change in frequency

For the coherence between the channels and the frequency, the absorption peaks of the five measurements were fitted to Gaussian curves. An example for such a fit can be seen in figure 13 For this, the data below the error threshold of the first dip was used, ignoring the others as results of relaxation effects. After this, the first dip was chosen as the reference to compute the absolute difference between this one and all the other ones. The resulting linear relationship between the change in channels for the change of frequency can be seen in figure 14. The parameters of the curve were $a = 0.000442 +/- 0.000020$ and $b = 0.004 +/- 0.005$ in a function $y = a \cdot x + b$.

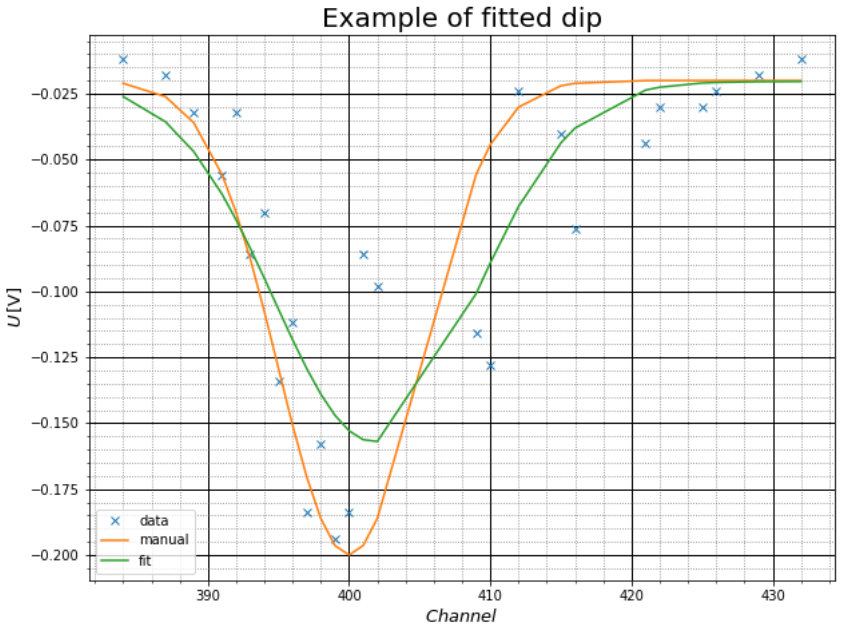

Figure 13: Plot of the data points of one absorption peak (dip) and the fitted Gaussian curve, as well a plot of the guessed starting parameters used for the fitted curve.

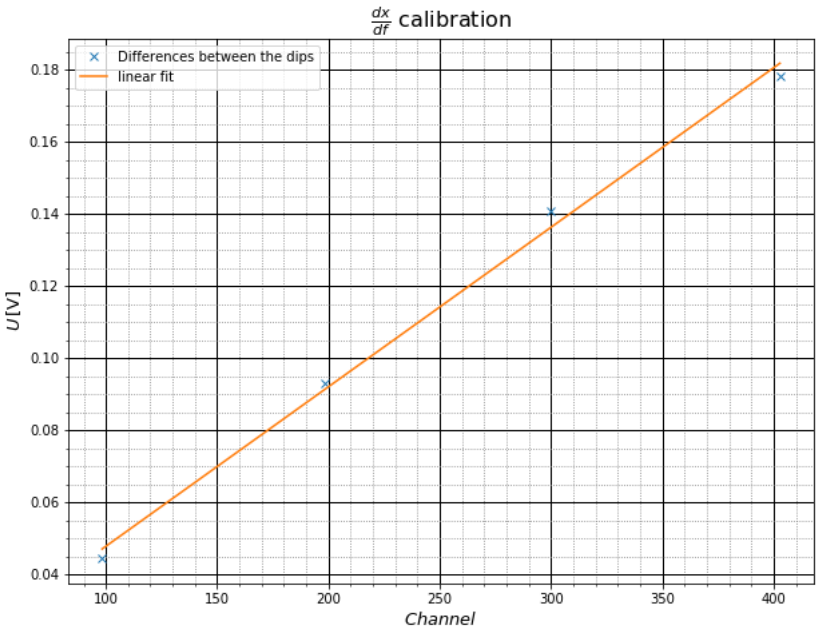

Figure 14: Plot of the change of channels per change of frequency data and the linear fit used later to compute the corrected resonance frequencies.

7.3 Computation of the resonance frequencies

With the computed error threshold and channel frequency relationship, the resonance frequencies of the different samples can be computed. An example of the data to be analysed is seen in figure 15. For this, the nullstellen of the magnetic field modifying sine wave were computed, utilizing a sine fit with `curve_fit`. This can be seen in the figure 16 Next, the resonance signal next to the nullstellen was analysed for the absorption maxima. Utilizing the error threshold, all values above were considered background and directly neighbouring points were considered signal. An example of the result of this procedure is seen in figure 17. From this points the first dip was analysed. Caused by the low sample number in the files, the original plan of fitting a Gaussian curve to each dip was not feasible. As a substitute, the minimum of each dip was chosen to be the recorded channel with the width of the entire dip as the error. Now, the distance between the dip and the closest nullstelle of the sine was computed for all dip-nullstellen pairs in the measurement and the mean of all distances was computed. This mean is the correction for the frequency at which the measurement was recorded. Utilizing the frequency channel relationship, the true resonance frequency of each measurement could be computed as the sum of the recorded frequency and the correction.

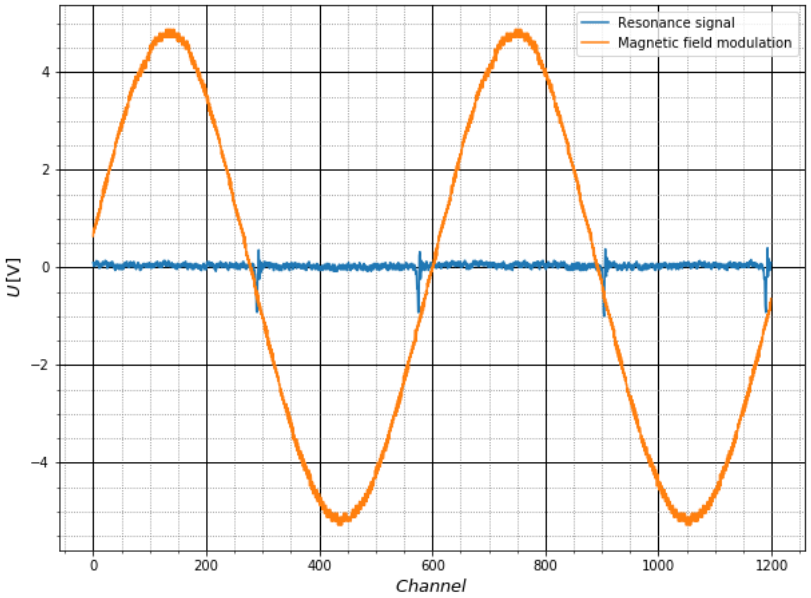

Figure 15: Example of the data recorded for one data point for one sample.

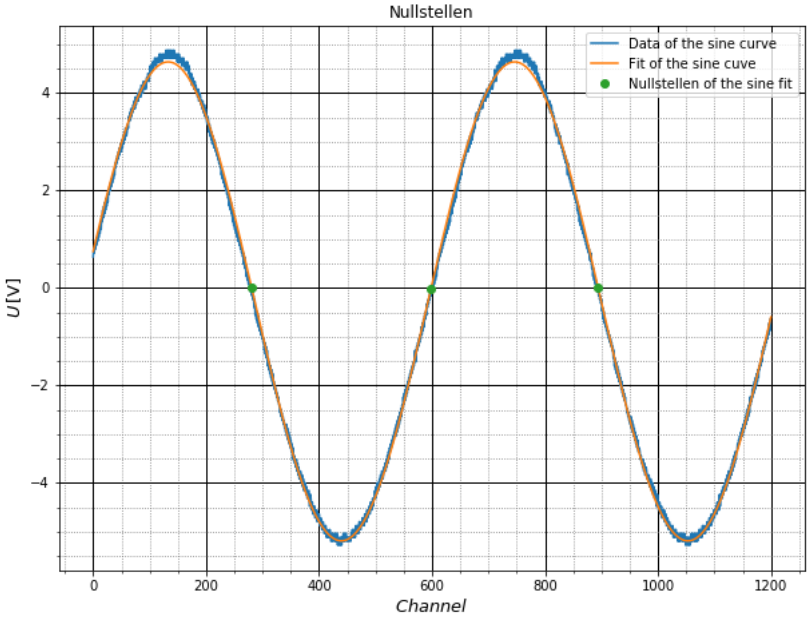

Figure 16: Example of the sine curve fitted to the data points of the modulation of the magnetic field. The nullstellen of the fit are marked.

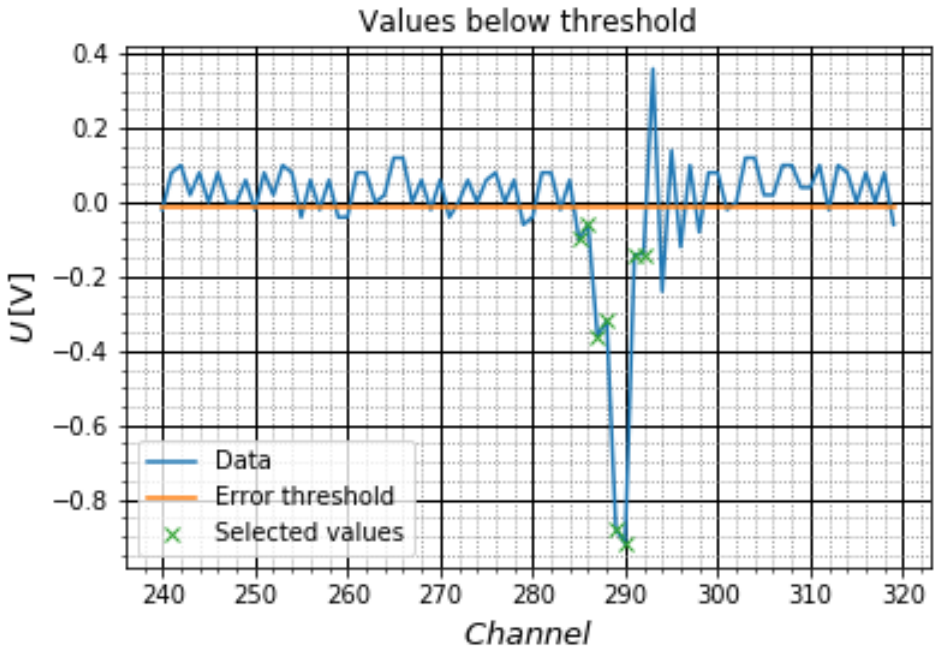

Figure 17: Example for the discrimination of the values used in the change of channel per change of frequency and resonance frequency calculation.

7.4 Computation of the nuclear magnetic momentum of ^{19}F

Using the corrected resonance frequencies and measured magnetic fields, the gyromagnetic ratio and nuclear magnetic momentum of ^{19}F were computed. Due to time dependent changes of the magnetic field, the error of the measured magnetic field was set to $\Delta B = 1\,\mathrm{mT}$. The resonance frequency has been corrected using the above steps. Utilizing the formular 4, formulas 8 and 9 could be deduced.

$$\gamma = 2\pi\frac{\nu_{res}}{B}; \qquad \Delta\gamma = \gamma\sqrt{\left(\frac{\delta\nu_{res}}{\nu_{res}}\right)^2 + \left(\frac{\Delta B}{B}\right)^2} \tag{8}$$

$$\mu_K = \gamma\hbar m_I = \frac{\gamma\hbar}{2}; \qquad \Delta\mu_K = \mu_K\left(\frac{\Delta\gamma}{\gamma}\right) \tag{9}$$

Table 1: Calculated results of ^{19}F

	Corrected resonance frequencies	Measured magnetic fields	γ	μ_K
0	19.096+/-0.006	461.0+/-1.0	0.2603+/-0.0006	(1.3724+/-0.0030)e-35
1	19.496+/-0.005	503.0+/-1.0	0.2435+/-0.0005	(1.2841+/-0.0026)e-35
2	18.524+/-0.006	474.0+/-1.0	0.2456+/-0.0005	(1.2948+/-0.0028)e-35
3	17.999+/-0.006	436.0+/-1.0	0.2594+/-0.0006	(1.3677+/-0.0032)e-35
4	17.548+/-0.006	447.0+/-1.0	0.2467+/-0.0006	(1.3006+/-0.0029)e-35
5	18.022+/-0.006	466.0+/-1.0	0.2430+/-0.0005	(1.2813+/-0.0028)e-35

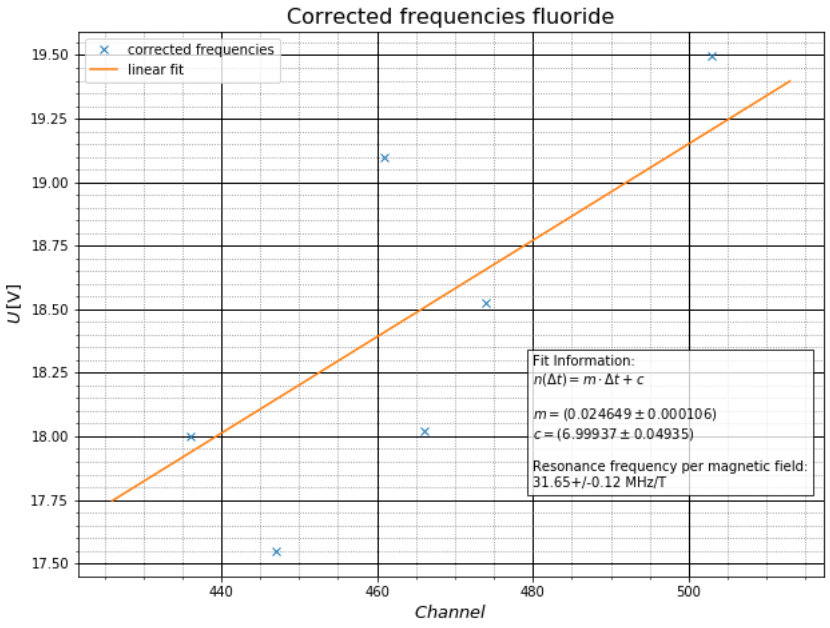

Figure 18: The resonance frequency of all the measurements with the Teflon sample with a linear fit to compute the relationship between the resonance frequency and the magnetic field for the ^{19}F nucleus. The measured relationship is listed in the figure.

7.5 Computation of the gyromagnetic ratio of the proton

Analogue to the previous calculation, the gyromagnetic ratio of the proton in glycol and hydrogen was computed with formular 8. The results are seen in table 2 for the glycol sample and table 3 for hydrogen.

Table 2: Calculated results of Glycol

	Corrected resonance frequencies [Mhz]	Measured magnetic fields [mT]	γ
0	18.577+/-0.006	395	(2.9550+/-0.0009)e+08
1	18.079+/-0.007	383	(2.9660+/-0.0012)e+08
2	17.520+/-0.006	371	(2.9671+/-0.0009)e+08
3	19.039+/-0.006	405	(2.9537+/-0.0009)e+08
4	19.492+/-0.006	414	(2.9582+/-0.0008)e+08

Table 3: Calculated results of hydrogen

	Corrected resonance frequencies [Mhz]	Measured magnetic fields [mT]	γ
0	19.560+/-0.006	414	(2.9686+/-0.0008)e+08
1	19.678+/-0.005	418	(2.9579+/-0.0008)e+08
2	19.002+/-0.006	404	(2.9552+/-0.0009)e+08
3	18.151+/-0.006	380	(3.0012+/-0.0009)e+08
4	17.519+/-0.006	371	(2.9670+/-0.0010)e+08
5	18.649+/-0.006	397	(2.9515+/-0.0009)e+08

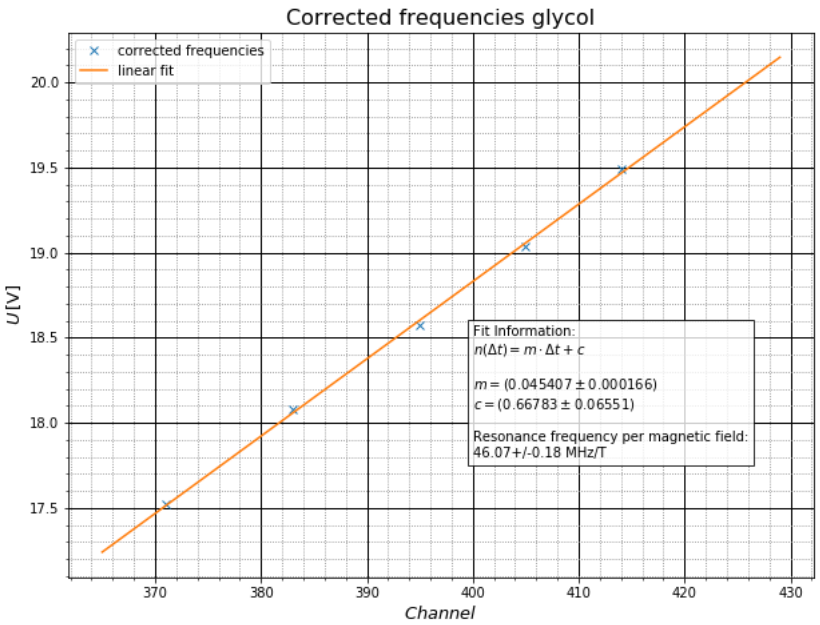

Figure 19: The resonance frequency of all the measurements with the glycol sample with a linear fit to compute the relationship between the resonance frequency and the magnetic field for the proton. The measured relationship is listed in the figure.

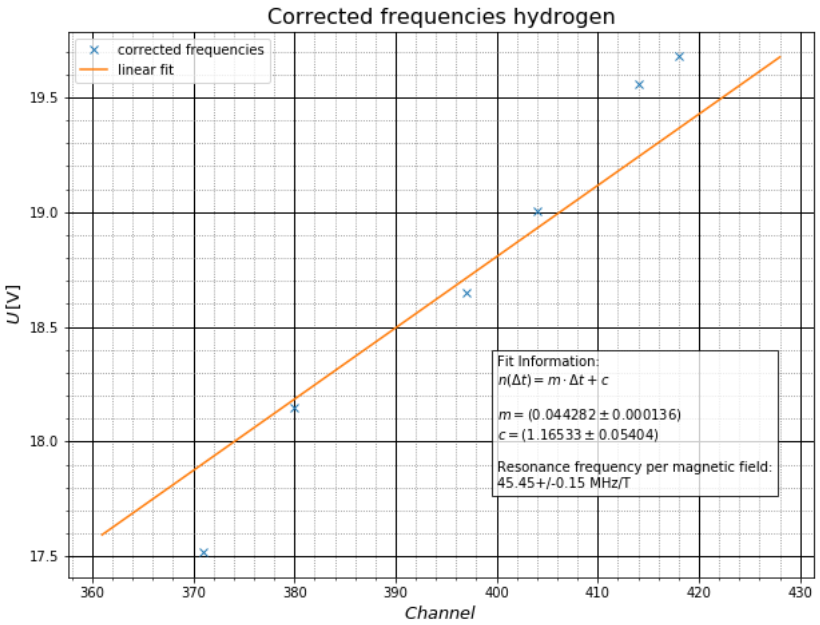

Figure 20: The resonance frequency of all the measurements with the hydrogen sample with a linear fit to compute the relationship between the resonance frequency and the magnetic field for the proton. The measured relationship is listed in the figure.

8 Analysis of the Lockin Method

For the analysis the 'Nulldurchgang' of both the Lock-In and the sawtooth signal needs to be calculated. First of all the slopes of the measured sawtooth were fitted with a linear fit of the form $f(x) = m \cdot x + b$. For the fit `curve_fit` of the python package `scipy.optimize` [4] was used. With these parameters the 'Nulldurchgang' for each measurement can be calculated. To do so equation 10 was used, with d_s being the position were the curve crosses zero. The error σ_{d_s} is calculated using Gaussian error propagation.

$$d_S = -\frac{b}{m} \tag{10}$$

$$\sigma_{d_S} = \sqrt{(\frac{\sigma_b}{m})^2 + (\frac{b}{m^2}\sigma_m)^2} \tag{11}$$

The parameters and 'Nulldurchgang' are documented in table 7. The figures of the measured signals as well as the corresponding fits can be seen for the data of the CSV file `lockin_9` in figure 21. The other ones can be found in the appendix in figure 24 to 29.

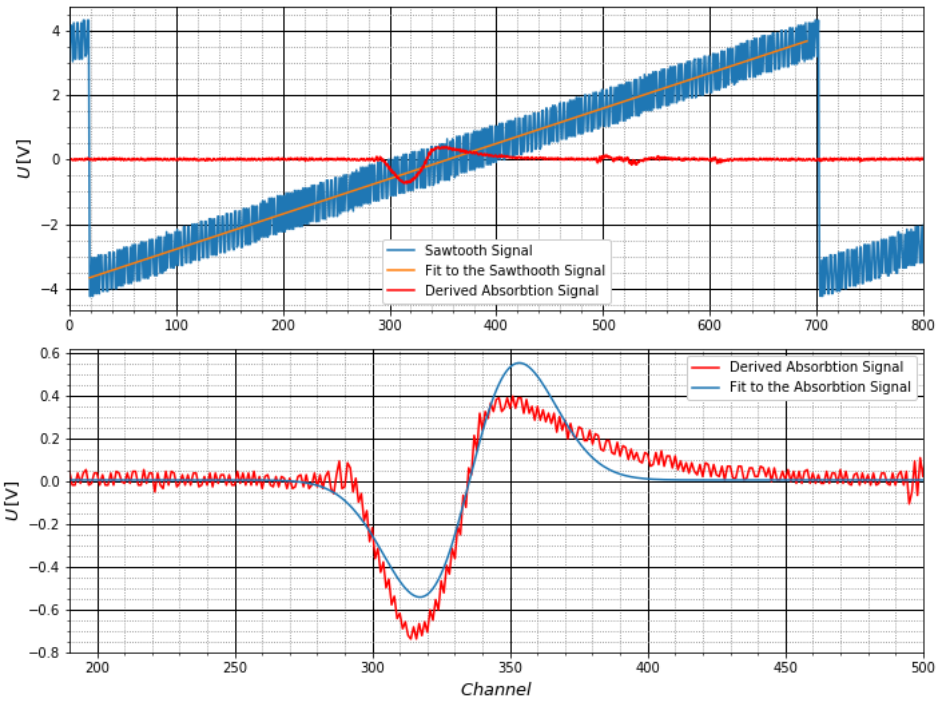

Figure 21: The upper figure shows the data of the sawtooth in blue with the corresponding fit in orange. The absorption signal is in red. The lower one shows the part of the absorption signal which is of interest with the fit in blue.

For the high frequency signal (HF) of the NMR Oscillator the derivative of an inverse Gaussian curve was fitted. The form can be seen in eq.12.

$$f(x) = \frac{a(x - d_A)e^{-\frac{(x-d_A)^2}{2c^2}}}{c^2} + h \tag{12}$$

As can be seen in figure 21 the fits aren't very similar to the measured data. The main problem is the asymmetry of the amplitudes which are different for the data but are expected to be similar in eq.12. The reason for this is very likely the Lock-In method as well as relaxation processes duo to which the expected Gaussian derivative is not a perfect match. The reason this fit was still used is that the needed parameter d_A which gives the 'Nullstelle' isn't affected to much. This can also be seen in table 8 since here the errors on the listed parameters d_A, which give the needed 'Nullstellen' position, aren't to high.

With those two positions of the sawtooth as well as the absorption signal the distance Δd between those can be calculated and depicted together with the corresponding frequency of the NMR Oscillator. The error for this gab $\sigma_{\Delta d}$ is calculated using eq.13.

$$\sigma_{\Delta d} = \sqrt{(d_A\sigma_{dS})^2 + (d_S\sigma_{dA})^2} \tag{13}$$

The data points were than fitted with the linear form $f(x) = m_2 \cdot x + b_2$. The difference to the sawtooth fit is, that the error $\sigma_{\Delta d}$ was used for this fit. Since `curve_fit` only takes errors of the y-axis, the errors for the frequency weren't used since they aren't as dominant for the calculation. The data points and the fit are shown in figure 22. The data points coloured in green were excluded from the fit calculation. The reason for this is warming up of the magnets and the long time between the measurement of these two points and the others. This caused a slow shifting in the magnetic field and with that a shift in the resonance frequency.

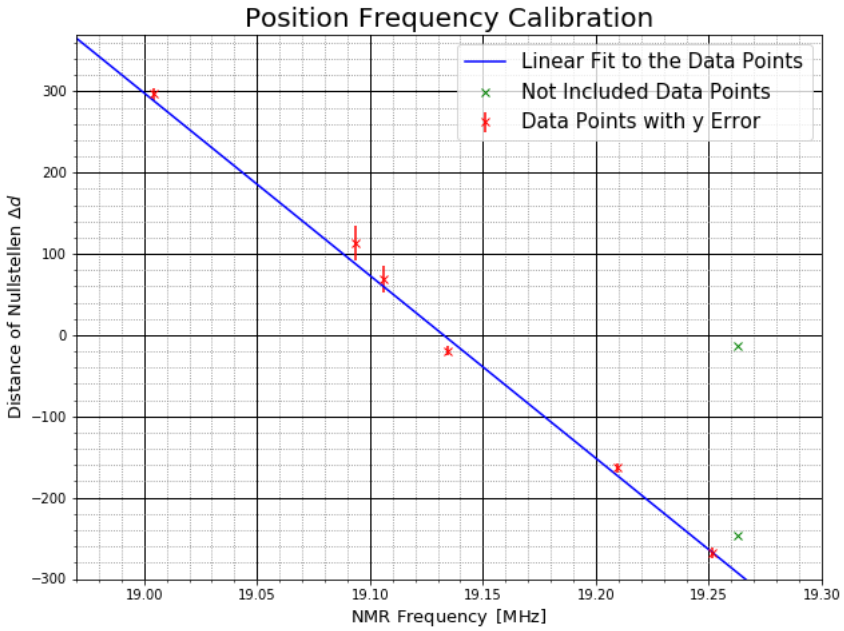

Figure 22: Plot of frequency against the distance Δd. The green data points were excluded from the fit calculation. The fit itself is calculated with the errors $\sigma_{\Delta d}$.

With the help of this fit the resonance frequency at which both 'Nullstellen' align can be found, since here the value for Δd is zero. Using equation 14 the frequency and its error were calculated.

$$f_{LockIn} = -\frac{b_2}{m_2} \tag{14}$$

$$\sigma_{d_S} = \sqrt{(\frac{\sigma_b}{m})^2 + (\frac{b}{m^2}\sigma_m)^2} \tag{15}$$

The resonance frequency for the Lock-In method we get using this calculation is:

$$f_{LockIn} = (19.1 \pm 0.6)\,\mathrm{MHz}$$

The corresponding magnetic field is calculated using the mean of the measured magnetic fields while the error is calculated using equation 16.

$$\sigma_x = \sqrt{\frac{1}{1-n}\sum_{n}^{i=1}(x_i - \bar{x})^2} \tag{16}$$

Here the first 3 measured B-fields were excluded. The reason for the first two is similar to the excluded data points in fig.22. The third one was excluded duo to its huge difference to the other values. The reason the difference is either that the sawtooth wasn't turned off, or the hall sensor was to long inside the magnetic field which increased the temperature. The problems with the Hall sensor are discussed in the conclusion. With that the magnetic field is at:

$$B_{LockIn} = (463.0 \pm 0.7)\,\mathrm{mT}$$

Table 4: Compatibility of the computed values for Teflon with the literature value

	compatibility
0	14.781406
1	17.031542
2	12.048958
3	12.547981
4	9.317133
5	16.816672

9 Discussion of the results

9.1 Hall Sensor

During the first part of the experiment (error and gyromagnetic ratio measurements), a different hall probe was used as during the rest of the experiment. While the first one did not have any obvious temperature dependency, the second one did clearly. Additional magnetic field measurements indicated this. Therefore, a bigger statistical and systematic error should be assumed for all measurements with the second hall probe. Nevertheless the possibility of a temperature dependency of the first hall probe should not be ignored.

9.2 Nuclear magnetic momentum of ^{19}F

The nuclear magnetic momentum (nmm) of ^{19}F was co compared with the literature value $\mu_K = 1.328 \cdot 10^{-26} \left[\frac{J}{T}\right]$ [3] utilizing equation 17. The results can be seen in table 4.

$$t = \frac{x_M - x_L iteratur}{\sigma_x} \tag{17}$$

As seen in the figure 18, the difference between the individual measurements of Teflon is big. Although the computed values for the nmm are in the range of the literature value, the errors are far too small, considering the problems with the measurement of the magnetic field with the new hall probe. There is also the issue with the number of points measured for the resonance frequency correction. Sometimes as few as 3 points were recorded per peak, which is very inaccurate. Therefore the measurement should, if repeated, be made with a higher number of samples or a smaller range. The comparison of the nuclear resonance frequency of the measurement ($\approx 31.65 \frac{MHz}{T}$, fig. 18) with the nuclear resonance frequency recorded in the manual ($40.06 \frac{MHz}{T}$, [2]), the difference is obvious. Therefore, the error from the measurement of the magnetic field should be dominant.

9.3 Gyromagnetic ratio

The literature value of the gyromagnetic ratio of the proton in glycol and hydrogen is $\gamma = 2.675 \cdot 10^8 \left[\frac{1}{sT}\right]$. With equation 17, the exact values for each measurement can be found for glycol in table **??** and for hydrogen in table 6.

Although the hall probe of these two measurements was more reliable, a temperature dependant error can not be excluded. When comparing the nuclear resonance frequencies of the measurements (glycol $\approx 46.07 \frac{MHz}{T}$, fig. 19; hydrogen $\approx 45.45 \frac{MHz}{T}$, fig.20) with the nuclear resonance frequency in the manual

Table 5: Compatibility of the computed values for glycol with the literature value

	compatibility
0	37.167007
1	37.160223
2	36.270509
3	37.954904
4	39.361233

Table 6: Compatibility of the computed values for hydrogen with the literature value

	compatibility
0	40.662869
1	39.709633
2	38.022509
3	41.010242
4	36.239995
5	36.936181

($42.58 \frac{MHz}{T}$ [2]), they appear quite close together. This means, the dominant error should be in the error calculation. Another source of errors is the low number of measurements as explained above.

9.4 Lock-in measurement

The lock-in measurement resulted in more accurate nuclear resonance frequency as the traditional methods. To compare this result with the literature value and the values of the other method, the ratio of the frequency over the magnetic field for the resonance was computed.

$$\frac{f_{LockIn}}{B_{LockIn}} = \frac{(19.1 \pm 0.6)\, MHz}{(463.0 \pm 0.7)\, mT} = (41.3 \pm 1.3), \frac{MHz}{T} \tag{18}$$

This is much closer to the reference value of $42.58 \frac{MHz}{T}$ [2]. The compatibility value of both is 1.02, so they are compatible with each other.

10 List of tables

List of Tables

11 List of Figures

List of Figures

12 Bibliograpy

References

[1] Manual of the electromagnets.

[2] *Versuchsanleitung: Fortgeschrittenen Praktikum Teil 1 Kernspin.*

[3] W. Demtröder. *Experimentalphysik Band 3: Atome, Moleküle und Festkörper.*

[4] Eric Jones, Travis Oliphant, Pearu Peterson, et al. Python3 package `scipy.optimize` for curve fitting., 2001–.

13 Appendix

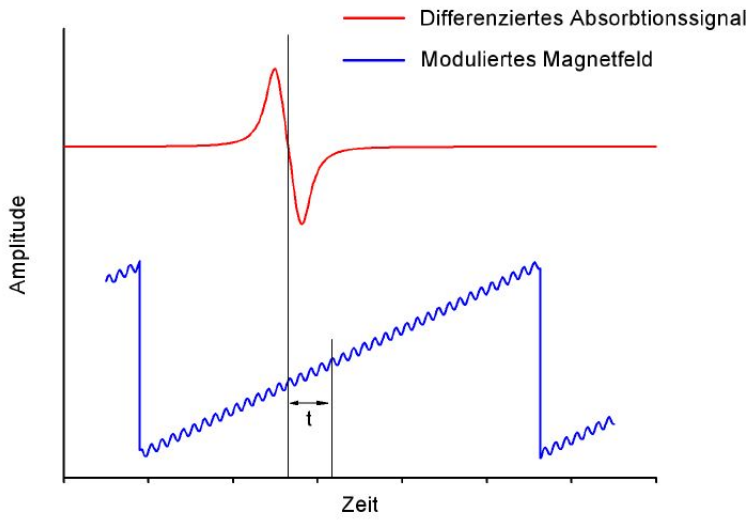

Figure 23: Derived absorption signal in red. Superposition of sinus and sawtooth waves with both 'Nulldurchgängen' aligned.[2]

CSV File	Parameter m	Parameter b	d_s
`lockin_2`	0.01090 ± 0.00011	-8.16 ± 0.08	748 ± 11
`lockin_3`	0.01091 ± 0.00011	-3.74 ± 0.04	1022 ± 22
`lockin_4`	0.01093 ± 0.00016	-11.16 ± 0.16	518 ± 8
`lockin_5`	0.01090 ± 0.00010	-5.65 ± 0.06	945 ± 17
`lockin_6`	0.01092 ± 0.00013	-10.32 ± 0.12	375 ± 6
`lockin_7`	0.01094 ± 0.00011	-4.10 ± 0.04	472 ± 7
`lockin_8`	0.01090 ± 0.00010	-5.14 ± 0.05	355 ± 5
`lockin_8`	0.01091 ± 0.00011	-3.87 ± 0.04	355 ± 5

Table 7: Parameters and position of the 'Nulldurchgang' of the sawtooth fit. Here m is the slope, b the crossing of the y-axis and d_s the 'Nulldurchgang'.

CSV File	a	d_A	c	h	Frequency[MHz]
`lockin_2`	16.3 ± 0.6	335.3 ± 0.5	18.0 ± 0.5	0.0076 ± 0.0035	19.2625 ± 0.00005
`lockin_3`	16.3 ± 0.6	203.6 ± 0.5	-18.8 ± 0.5	0.0072 ± 0.0035	19.2629 ± 0.00005
`lockin_4`	16.6 ± 0.6	211.6 ± 0.5	18.9 ± 0.5	0.0082 ± 0.0035	19.0935 ± 0.00005
`lockin_5`	15.7 ± 0.6	1014.0 ± 0.5	18.2 ± 0.5	0.0086 ± 0.0034	19.0041 ± 0.00005
`lockin_6`	16.7 ± 0.5	814.9 ± 0.5	17.0 ± 0.5	0.0077 ± 0.0034	19.1063 ± 0.00005
`lockin_7`	15.3 ± 0.6	1134.8 ± 0.5	17.1 ± 0.5	0.0050 ± 0.0035	19.2091 ± 0.00005
`lockin_8`	16.7 ± 0.5	97.0 ± 0.5	-18.5 ± 0.5	0.0078 ± 0.0032	19.2518 ± 0.00005
`lockin_8`	16.4 ± 0.6	734.6 ± 0.5	18.4 ± 0.5	0.0072 ± 0.0035	19.1344 ± 0.00005

Table 8: Parameters and position of the 'Nulldurchgang' of the derived Gaussian fit.

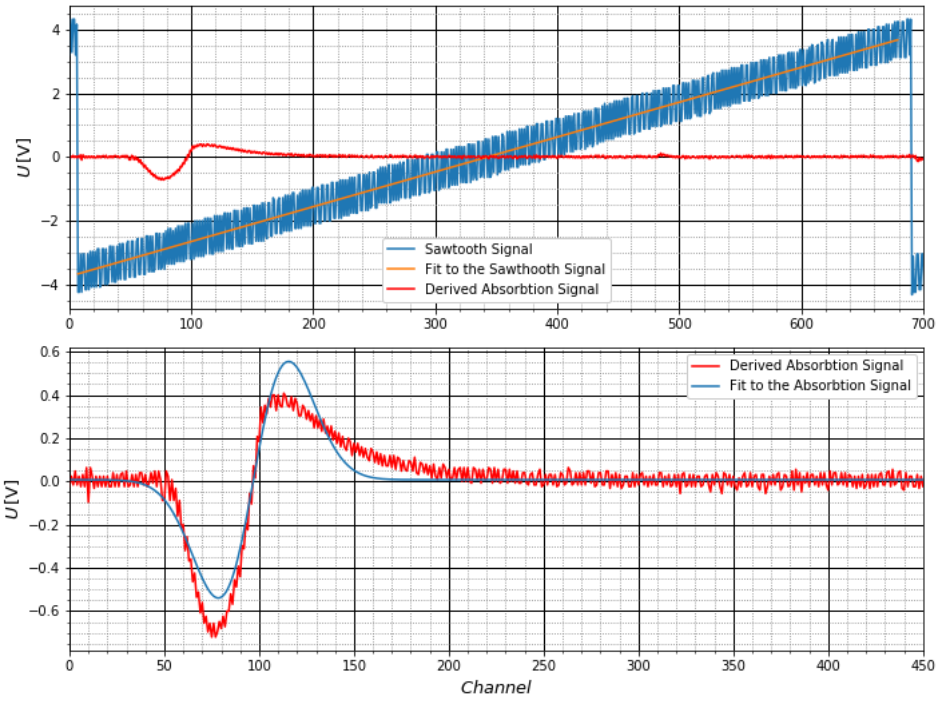

Figure 24: The upper figure shows the data of the sawtooth in blue with the corresponding fit in orange. The absorption signal is in red. The lower one shows the part of the absorption signal which is of interest with the fit in blue. This figure is of the CSV file lockin 2.

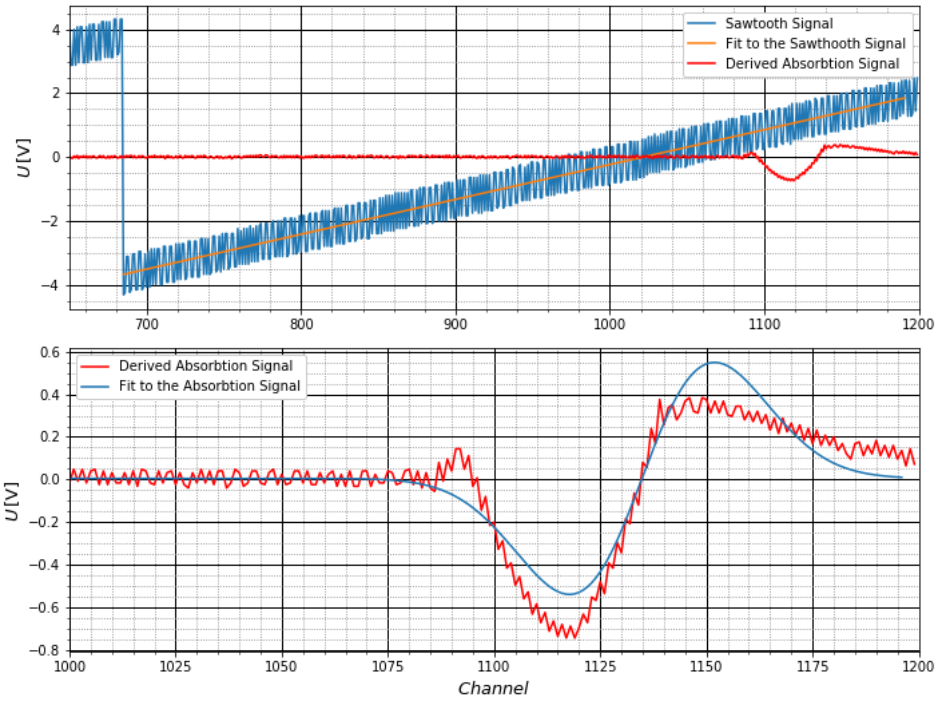

Figure 25: The upper figure shows the data of the sawtooth in blue with the corresponding fit in orange. The absorption signal is in red. The lower one shows the part of the absorption signal which is of interest with the fit in blue. This figure is of the CSV file lockin 3.

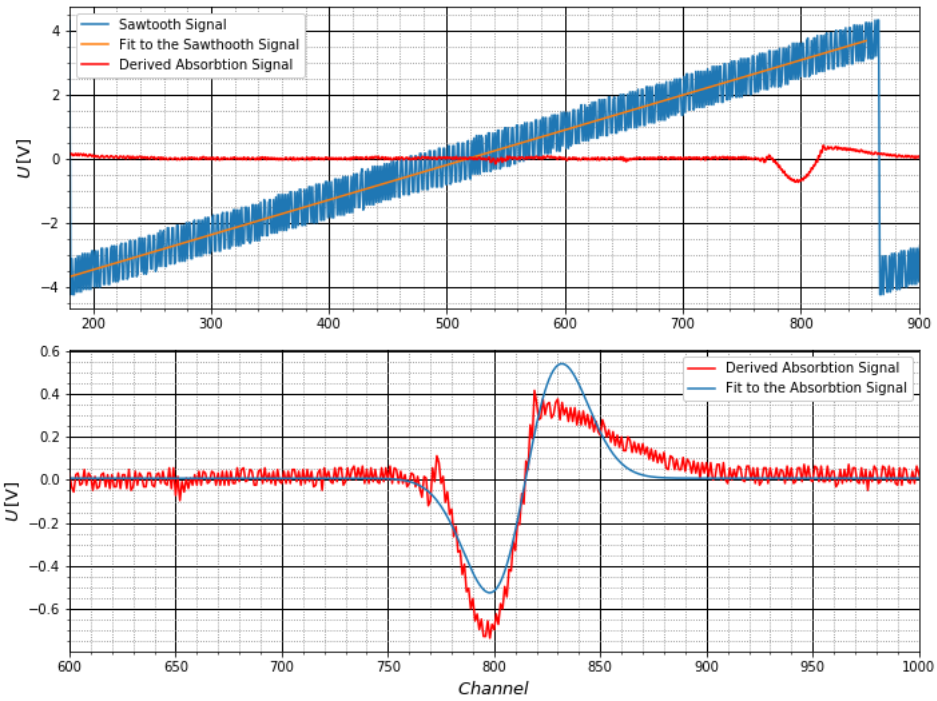

Figure 26: The upper figure shows the data of the sawtooth in blue with the corresponding fit in orange. The absorption signal is in red. The lower one shows the part of the absorption signal which is of interest with the fit in blue. This figure is of the CSV file lockin 4.

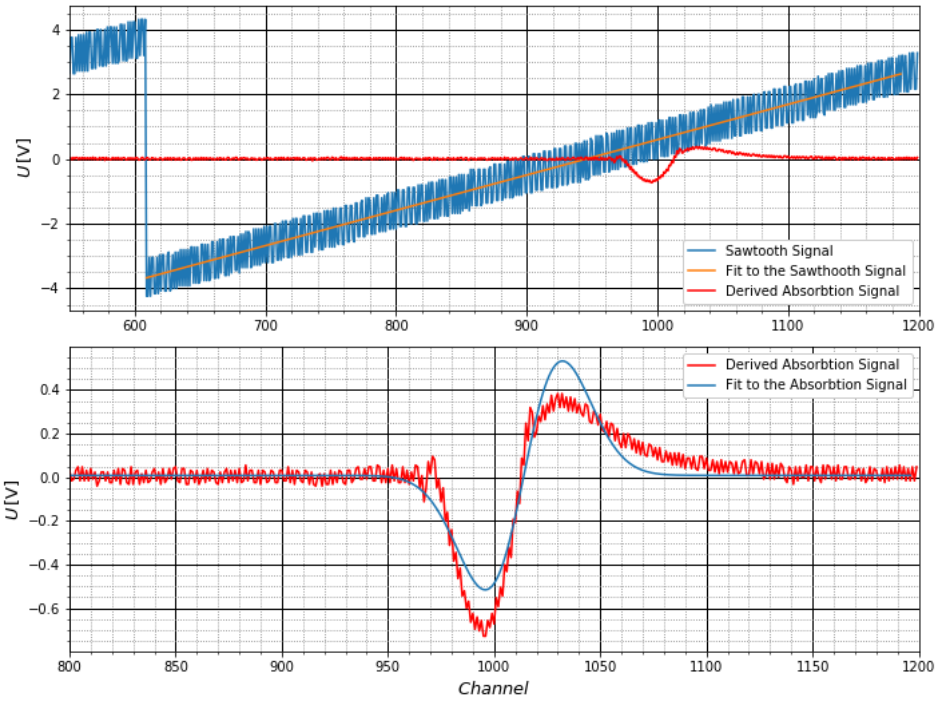

Figure 27: The upper figure shows the data of the sawtooth in blue with the corresponding fit in orange. The absorption signal is in red. The lower one shows the part of the absorption signal which is of interest with the fit in blue. This figure is of the CSV file lockin 5.

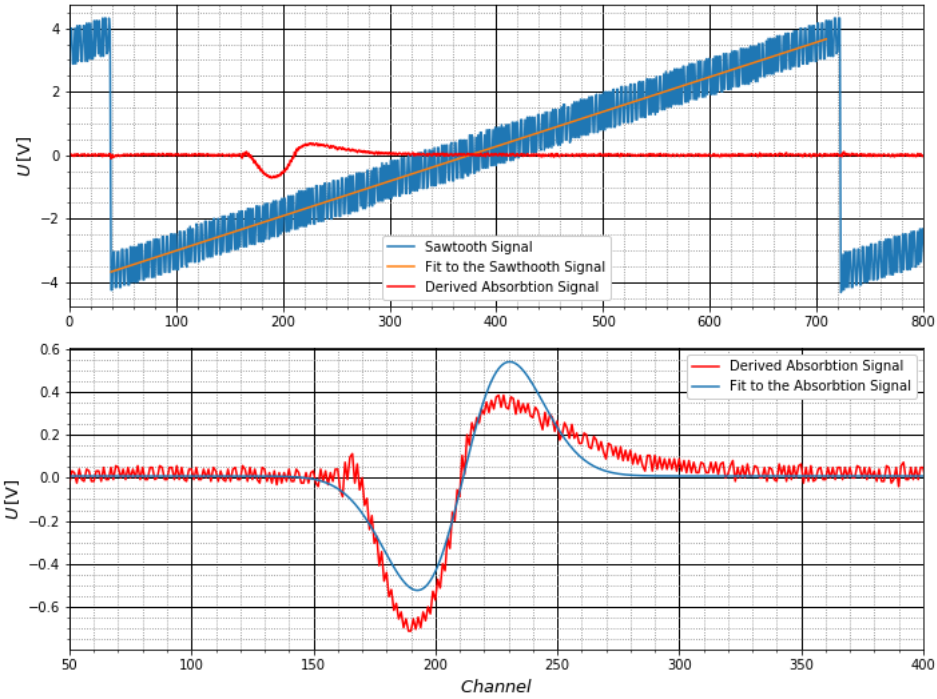

Figure 28: The upper figure shows the data of the sawtooth in blue with the corresponding fit in orange. The absorption signal is in red. The lower one shows the part of the absorption signal which is of interest with the fit in blue. This figure is of the CSV file lockin 6.

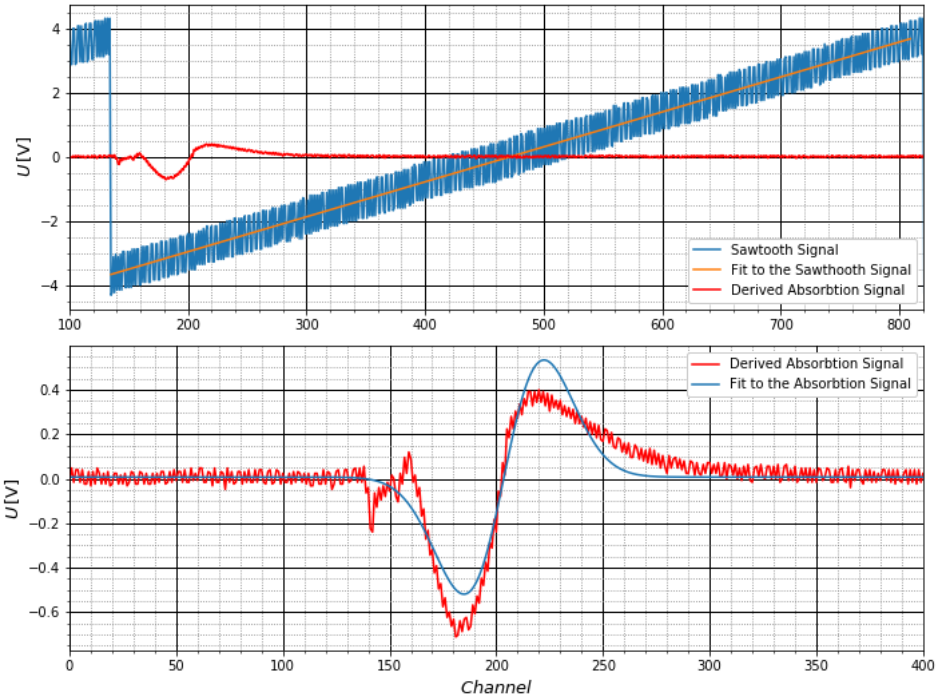

Figure 29: The upper figure shows the data of the sawtooth in blue with the corresponding fit in orange. The absorption signal is in red. The lower one shows the part of the absorption signal which is of interest with the fit in blue. This figure is of the CSV file lockin 7.